PCCP

Accepted Manuscript

ROYAL SOCIETY OF CHEMISTRY

www.rsc.org/pccp

Formation of a thermally stable bilayer of coadsorbed intact and deprotonated thymine exploiting the surface corrugation of rutile TiO_2(110)†

D. A. Duncan[1, 2], J. H. K. Pfisterer[1], P. S. Deimel[1], R. G. Acres[3ŧ], M. Fritton[4], P. Feulner[1], J. V. Barth[1] and F. Allegretti[1]*

[1] Physik-Department E20, Technische Universität München, D-85748 Garching, Germany

[2] Diamond Light Source, Didcot, Oxfordshire OX11 0DE, UK

[3] Elettra-Sincrotrone Trieste, Strada Statale, 34149 Basovizza, Trieste, Italy

[4] Deutsches Museum, Museumsinsel 1, D-80538 München, Germany

* Email: francesco.allegretti@ph.tum.de

ŧ Present address: Australian Synchrotron, 800 Blackburn Road, Clayton, Victoria, 3168, Australia.

† Electronic supplementary information (ESI) available.

Abstract

The adsorption of thymine, a pyrimidine based nucleobase, was studied on the (110) termination of rutile titanium dioxide in order to understand the thermal stability and gross structural parameters of the interaction between a strongly polar adsorbate and a highly corrugated transition metal oxide surface. Near-edge X-ray absorption fine structure (NEXAFS), X-ray photoelectron spectroscopy (XPS), temperature programmed XPS and temperature programmed desorption indicated the growth of a room temperature stable bilayer, which could only be removed by annealing to 450 K. The remaining first layer was remarkably robust, surviving annealing up to 550 K before undergoing N-H bond scission. The comparison to XPS of a sub-monolayer exposure of 1-methyluracil shows that the origin of the room temperature stable bilayer is not intermolecular interactions. This discovery, alongside the deprotonation of one of the first layer's pyrimidinic nitrogen atoms at room temperature, suggests that the thymine molecules in the first layer bind to the undercoordinated surface Ti atoms, and the second layer thymine molecules coordinate with the bridging oxygen atoms which protrude above the Ti surface plane on the (110) surface. The NEXAFS results indicate an almost upright orientation of the molecules in both layers, with a 30 ± 10° tilt away from the surface normal.

1. Introduction

The study of simple biomolecules (and molecules inspired by them) on titanium dioxide has often been motivated by the prominence of titanium in bioimplants[1-10] and the fact that a 3–100 nm thick oxide layer readily forms on implanted titanium metal at ambient conditions (both in air and in aqueous environment).[1, 11-14] However, even beyond the desire to better integrate bioimplants by functionalizing the oxidized surface of titanium, the (110) rutile substrate provides an intriguing corrugation that is not often found on well-characterised surfaces. On the (110) rutile surface, going across the [1$\bar{1}$0] direction, alternating rows of undercoordinated titanium and oxygen atoms which do not share the same geometric plane are found.[15] This creates not only a geometric corrugation, with protruding rows of bridging oxygen atoms (O_b) and adjacent Ti-exposing (fivefold Ti, 5-Ti) troughs running along the [001] substrate direction, but a corrugation in the effective charge of the surface atoms as well (formally Ti^{4+} / O^{2-}, theoretically $Ti^{1.7+}$ / $O^{0.85-}$ in Ref. [16], and more specifically $Ti^{1.5+}$ / $O^{0.6-}$ for the 5-Ti and O_b atoms on the surface[17]). The ability of TiO_2(110) to act one-dimensionally has often been observed[18-20] as a result of the highly corrugated potential-energy profile, and it can be exploited to pattern molecular adsorbates on its surface.[21-26] The adsorption of such species is usually mediated by the positively biased undercoordinated surface Ti atoms[7, 21, 27-32].

Nucleobases are molecular species which, in their biological role, are involved in strong hydrogen bonding, both in forming a base pair (cf. DNA) and interacting with the amino acid chains which they encode. They possess dipole moments in the range of 2.5–7 D,[33] and therefore they are intrinsically polar.[34, 35] As such, they provide an interesting class of molecules to introduce to a highly corrugated substrate like rutile TiO_2(110) and could be expected to interact with either the surface oxygen atoms or the surface metal atoms. Notably, titania nanoparticles have been used as a hole injector to adsorbed short-chain DNA molecules as a method to "read" the DNA sequence.[36] The DNA molecules were anchored using a dopamine linker, therefore utilising a key component of DNA, such as a nucleobase, could provide a more natural anchoring of DNA for such device applications. The adsorption of nucleobases on the TiO_2(110) substrate may also be broadly compared to the adsorption on the (110) surface of fcc crystals, which have a similar, though much weaker, geometric and electronic corrugation.[37, 38] On the (110) surface of Cu, specifically, thymine,[39, 40] uracil[41] and cytosine[42] (the three pyrimidine based, and therefore simplest, nucleobases) were all observed to adsorb upright, aligned mostly along the close-packed direction (the [1$\bar{1}$0] direction in fcc(110) substrates) with one of the pyrimidine N atoms and the carbonyl oxygen atom(s) in off atop chemisorbed sites. As carboxylate species on both Cu(110)[43-45] and TiO_2(110)[7, 27] adsorb in broadly comparable sites (near atop metal surface atoms), the expectation would be that nucleobases would also adsorb in similar sites through one of their N atoms.

With this in mind, we have studied the adsorption of thymine on the (110) termination of rutile TiO_2

using synchrotron X-ray photoelectron spectroscopy (SXPS), lab-source X-ray photoelectron spectroscopy (XPS), near-edge X-ray absorption fine structure (NEXAFS), temperature programmed XPS (TP-XPS) and temperature programmed desorption (TPD) in order to understand the chemical and electronic environment of adsorbed thymine, as well as its thermal stability. To our knowledge, this is the first study of nucleobases adsorbed on well-defined single-crystal oxide surfaces; its findings are therefore expected to deliver both novel and fundamental insights regarding the increase of complexity of the nucleobase/substrate interaction compared to the case of the most studied noble metal surfaces. Moreover, the elucidation of the interfacial interaction of one of the simplest biomolecules with a model oxide surface from a rigorous surface science perspective may represent an important as well as necessary step for tailoring the biofunctionalization of oxide nanoparticles and nanocomposites, a promising approach currently used in primary biomedical applications, such as cancer diagnostics, antitumor therapy and targeted drug delivery. [46-53]

2. Experimental Details

All ultra-high-vacuum (UHV) chambers utilized in the experiments were equipped with the standard facilities for sputtering (Ar gas, 0.5 keV), annealing (950-1050 K) and deposition of molecular layers; characterization of the surface quality by means of a low energy electron diffraction (LEED) apparatus was also possible. TiO_2(110) single crystals of square shape (10 mm × 10 mm), purchased from PI-KEM Ltd., were used as substrates. All samples were mounted on a Mo backplate to provide more even heating across the crystal. In the synchrotron experiments, this was achieved by mechanically clamping the sample onto the backplate. In the TP-XPS and TPD experiments, due to the larger sampling area of the lab based measurements and in order to prevent spurious desorption signals from the clips, mechanical clamping was avoided and the TiO_2 crystal was mounted using Aremco Ceramabond 503 alumina thermal glue. The latter was mixed in a 20:1 mass ratio with carbon black in order to make it conductive.[54] The mixture was applied between the Mo backplate and the back of the TiO_2 crystal before being annealed to 370 K in air for one hour, and to 570 K in high vacuum for one hour.

As to the synchrotron experiments, SXPS and NEXAFS measurements were performed at the Materials Science beam line on a bending magnet at the Elettra Light Source (Trieste, Italy) and at the I311 undulator beam line at the Max II Laboratory (Lund, Sweden). The base pressure of the measurement chamber was 2×10^{-10} mbar in both end stations. The Materials Science end station is equipped with a SPECS PHOIBOS 150 hemispherical electron energy analyser; it allows rotating the sample around a vertical axis in the surface plane to vary the incidence angle of the incoming photons, and around the surface normal to vary the surface azimuth the linear polarization of the light (horizontal) was aligned with. The I311 end station is equipped with a Scienta SES200 hemispherical

electron energy analyser. The NEXAFS spectra at the bending magnet beam line were recorded in the Auger yield mode, detecting the C KLL and N KLL decay electrons in the kinetic energy range of 225-275 eV and 355-395 eV, respectively. In order to rule out possible effects from beam damage, relevant core levels were frequently monitored by SXPS between successive NEXAFS scans, and the sample was moved laterally before acquiring a new spectrum. Strictly, beam damage on a time scale much quicker than our SXPS acquisition times cannot be excluded. However, the consistency of XPS data taken at a bending magnet beam line, an undulator beam line and with a standard lab source (see below), namely with photon intensities differing by several orders of magnitude, strongly suggests that the observed features were not influenced by beam damage.

The TP-XPS and TPD measurements were acquired on a home built chamber mounted at the E20 chair of the TU Munich (Garching, Germany). A SPECS PHOIBOS 100 CCD analyser and a twin-anode X-ray tube, of which the Mg Kα (hν = 1253.6 eV) radiation was utilised for the TP-XPS measurements, whereas a quadrupolar mass spectrometer fitted with a liquid nitrogen cooled cup over the ionizer[55] was employed for the TPD experiments. The temperature was monitored by a thermocouple mounted between the crystal and the Mo back plate and controlled precisely using a home built proportional–integral–derivative (PID) controller.

The binding energy scale of the XP spectra was calibrated using the literature value (459.3 eV)[56, 57] for the binding energy of the Ti $2p_{3/2}$ core level (lab-based experiments, N 1s and O 1s spectra in the synchrotron measurements), or the corresponding value (37. 5 eV)[57] for the shallower Ti 3p core level (synchrotron-based C 1s spectra).

In-situ preparation of TiO_2(110)(1×1) involved repeated cycles of Ar^+ sputtering and UHV annealing (950-1050 K).[58] This procedure typically leaves a percentage of bridging oxygen vacancies on the surface (up to ~5-10%), [15, 29, 59] which in the case of a small residual pressure of water in the UHV chamber are readily saturated with bridging hydroxyls.[58] The reproducibility of the preparation procedure, the cleanliness and defect states were checked by XPS and valence band photoemission, at the synchrotron, and by XPS and H_2O TPD experiments in our TUM facility and compared to literature data.[15] Thymine (Sigma-Aldrich, ≥ 99%) was sublimated by heating the powder within the crucible of an organic molecular beam evaporator up to 380 K. 1-methyluracil (Sigma-Aldrich, 99%) was evaporated using a specially built directional needle-doser that allows mild heating for molecular species that sublime at comparatively low temperatures. It consisted of a stainless steel tube that extended into the UHV chamber and was directly heated by passing an AC current through an electronically isolated K-type thermocouple wire going along the length of the tube (covered by a copper shroud to evenly spread the heat) and spot welded to the tube near its end; the temperature was measured by monitoring the DC voltage across the thermocouple. The tube was then attached, through a UHV feedthrough, to a stainless steel cross piece that contained the molecular powder and

could be heated externally by a heating tape with the temperature monitored by an externally mounted K-type thermocouple. Through this method, 1-methyluracil was evaporated at 370 K, keeping both the cross piece and the tube at this temperature for the period of exposure.

3. Results

3.1 Thymine/TiO_2(110): temperature evolution by XPS

Under a saturation exposure of thymine at room temperature two clear peaks in the N 1s SXPS were observed (Fig 1a). These peaks were assigned, similarly to previous work on Cu(110),[39, 41] to nitrogen atoms that have been deprotonated by coordination to surface metal atoms (at a binding energy of 399.5 eV) and protonated nitrogen atoms that are not directly coordinated to a surface metal atom (at a binding energy of 401.3 eV). After room temperature deposition an approximate 3:1 ratio was observed between these two species, which reduced to a 1:1 ratio after annealing to 450 K. Subsequent annealing to 550 K almost completely removed the feature at 401.3 eV (assigned to the protonated N). The corresponding changes in the C 1s core-level spectra are also shown in Fig 1c. Monitoring the N 1s core level as a function of temperature via TP-XPS reveals a rapid decrease in the intensity of the 401.3 eV feature between 300 and 450 K, corresponding to a significant desorption rate of mass 55 amu, a major cracking fragment of thymine,[60] in TPD. The 401.3 eV feature then shows a second, more gradual, decrease between 450 K and 550 K, which is not associated with any mass 55 amu desorption. Conversely, between 300 and 450 K the 399.5 eV feature shows only muted increases in intensity, but a more rapid increase between 450 K and 550 K. Above 550 K, the 399.5 eV feature slowly reduces in intensity, without a subsequent increase in intensity at another binding energy.

Comparing N 1s and Ti 2p SXPS data measured sequentially at the same photon energy (hv = 550 eV) after annealing to 450 K, assuming an inelastic mean free path through the TiO_2 of 0.3 nm (extrapolated from Ref.[61]), a negligible attenuation by the molecular adlayer, and a N 1s and Ti 2p photoionization cross section of 0.34 and 1.47 Mbarn (respectively),[62] then the apparent coverage is estimated to be 0.15 ML (where 1 ML is defined as one molecule per TiO_2(110) surface unit mesh of area 0.649×0.296 nm^2) or ~0.75 thymine molecules per nm^2. This would in turn suggest a total coverage after saturation exposure at room temperature of 0.3 ML or ~1.5 thymine molecules per nm^2. However, in addition to ignoring any possible difference between the attenuation of the thymine and the surface oxygen atoms, this crude estimate also ignores possible effects from photoelectron diffraction and differences in the transmission function of the electron analyser as a function of kinetic energy, and it should thus be considered with great caution.

3.2 Thymine/TiO_2(110): molecular orientation by NEXAFS

The angle-dependent N K-edge and C K-edge NEXAFS signatures of thymine on TiO_2(110), subsequent to annealing to 450 K, are displayed in Fig 2. The N K-edge NEXAFS shows two sharp pre-edge features, which are assigned to the two different initial states that correspond to the two core-level peaks in the N 1s SXPS (the absorption peak at lower photon energy is attributed to the photoemission peak at lower binding energy). Specifically, the two resonances originate from a transition from the respective N 1s core level into the lowest lying π* anti-bonding state. Similarly, the C K-edge NEXAFS shows four sharp pre-edge features, which are also predominantly assigned to the transitions from the four chemically shifted C 1s core-level features into the lowest lying π* orbital.[63] Both absorption edges show a significant dichroism between the photon polarization along the surface plane (Θ = 90°) and the photon polarization mostly along the surface normal (Θ = 20°). Importantly, a comparable dichroism is also seen, in the Θ = 90° geometry, between the incident photon polarization along the $[1\bar{1}0]$ azimuth, and the [001] azimuth. In addition, a similar angular dependence is observed in Fig 3, which contains the N K-edge and C K-edge NEXAFS after annealing to 550 K. This suggests that the plane of the aromatic ring of adsorbed thymine, after annealing to 450 K and 550 K, is similarly orientated mostly along the [001] direction in an upright geometry (mostly parallel to the surface normal). As shown in Table 1, the quantitative results of fitting both spectra according to established procedures,[64, 65] indicate a tilt of the molecule of 30 ± 10° with respect to the surface normal and a rotation (twist) of 30 ± 10° with respect to the [001] direction.

Conversely, the 300 K spectrum, recorded after saturation exposure of TiO_2(110) to thymine, displays a differing dichroism for the two observed N K-edge NEXAFS resonances (Fig 4a). The lower photon energy feature, relating to the lower binding energy N 1s SXPS peak, has a similar dichroism to that seen after annealing to 450 and 550 K. In contrast, the higher photon energy resonance, corresponding to the higher binding energy component in N 1s SXPS , exhibits a similar angular dependence between 90° and 20° as the lower binding energy species, but it shows almost no dichroism between the $[1\bar{1}0]$ and [001] azimuths. This suggests that, although the lower and higher photon energy peaks relate to a similar tilt with respect to the surface normal, there is a different rotation of the molecular plane around the surface normal. The higher photon energy peak suggests a rotation of 40 ± 10° with respect to the [001] direction. However, if the higher photon energy peak is assumed to have a contribution from two distinct species, specifically, one species that is in the same plane as that described by the lower photon energy peak, with the same ratio of intensities as seen in Fig 2, and a second species in a different plane, then the resulting quantitative fit suggests that the second species has a twist of 50 ± 15° with respect to the [001] direction.

3.3 Thymine/TiO_2(110) vs. 1-methyluracil/TiO_2(110): chemical characterization by N 1s XPS

We have also performed SXPS measurements after a sub-monolayer exposure to thymine (Fig 5a, left). Here, the N 1s core-level spectrum comprises a higher binding energy component that is significantly more intense than the lower binding energy feature (this time with an intensity ratio closer to 2:1 than to 3:1). Similarly to the previous analysis, after annealing to 450 K the higher binding energy feature decreases in intensity, with the intensity ratio of the two peaks moving towards 1:1. Comparing this N 1s SXPS of a sub-monolayer of thymine to N 1s XPS (Fig 5b) for a similar coverage of 1-methyl-uracil, then a very similar line shape is observed. Finally, we performed an additional test experiment where a saturated layer of thymine was annealed to 600 K (causing deprotonation of both N atoms) and subsequently re-exposed to thymine at room temperature up to saturation. In this case, N 1s XPS shows a near 1:1 ratio of the two N 1s components (Fig 5a, right).

4. Discussion

After deposition of thymine at 300 K, the approximate 3:1 intensity ratio for the two nitrogen species (Fig 1, SXPS) suggests that either half of all thymine molecules have one deprotonated nitrogen and the other half have two protonated nitrogen atoms, or alternatively, a quarter of the all thymine molecules have both nitrogen atoms deprotonated and three quarters have both nitrogen atoms protonated. In addition, a similar ratio of deprotonated to protonated N atoms was observed for a sub-monolayer coverage, suggesting that, regardless of the interpretation, a mixture of (partially or fully) deprotonated and fully protonated thymine molecules exist on the surface after deposition at room temperature. The combination of the N 1s TP-XPS, the mass 55 amu TPD spectrum (Fig 1) and N 1s SXPS of a fully deprotonated layer re-exposed to thymine (Fig 5b, right), however, strongly suggests that the first interpretation is more likely, and that the fully protonated thymine molecules desorb at a temperature between 300 K and 450 K. This, in turn, indicates that there are two thymine species, one that is strongly bound to the substrate with one of its nitrogen atoms deprotonated, and one that is stable at room temperature, but ultimately less strongly bound, with both of its nitrogen atoms protonated. We therefore propose that upon saturation exposure of thymine at 300 K a bilayer structure forms, i.e. an overlayer consisting of two saturated adsorption sites. The first layer comprises a strongly bound singly deprotonated species, and the second layer a more weakly bound protonated species. Specifically, we propose that the coordination of the more strongly bound layer to a Ti surface atom induces the deprotonation (first layer thymine species), and that the less strongly bound layer is either adsorbed on top of the first layer or coordinated to a surface oxygen atom (second layer thymine species). It then follows that after annealing to 450 K and 550 K only the first layer remains, in the latter case with also the second nitrogen atom thermally deprotonated by annealing. Furthermore, after deposition at 300 K the surface is covered in both the first and second

layer, with the higher binding energy peak (in the N 1s SXPS and XPS) that corresponds to the protonated N species having around a 1/3rd contribution from the first layer thymine and a 2/3rd contribution from the second layer thymine, and the lower binding energy peak that corresponds to the deprotonated N species having a contribution solely from the first layer thymine.

As observed in Fig 5a (left), not only does the second layer exhibit relatively high thermal stability, it also seems to be energetically favourable as it forms before a saturated first layer is complete. Despite the total coverage being 45% of the bilayer coverage (specifically, the lower binding energy peak having 70% of its saturated intensity), the higher binding energy peak is still over double the intensity of the lower one. Therefore, the formation of the second layer is either more energetically favourable than a denser packing of the first layer, or, once the thymine molecule is in its second layer adsorption site, it does not have enough energy at 300 K to overcome the activation barrier to reach a first layer site. The latter interpretation is perhaps more likely as, after annealing this layer to 450 K, the lower binding energy peak increases in intensity. Although this could be explained by less attenuation due to desorption of a small fraction of the second layer, it can also be reconciled with some of the second layer molecules finding free first layer sites on the substrate.

From the C and N K-edge NEXAFS after annealing to 450 K and 550 K (Figs 2 and 3, respectively) it is found that the first layer is mostly aligned along the [001] direction (with a twist of 30 ± 10°) and mostly parallel to the surface normal (with a tilt of 30 ± 10°). This orientation of the molecular plane in the first layer also seems to be true prior to annealing (after deposition at 300 K), as shown by the behaviour of the lower photon energy peak of the N K-edge NEXAFS (Fig 4). The second layer also displays a similar orientation relative to the surface normal, as observed in the higher photon energy peak (Fig 4), but it is less aligned along the [001]. In order to deconvolute the first and second layer contributions to this higher photon energy peak, we have assumed that the intensity of the first layer contribution will have a similar absorption profile as the 450 K annealed layer (Fig 2). In other words: the ratio of the first layer's contribution to the lower and higher photon energy peak will be the same as that observed for 450 K, and any remaining intensity in the N K-edge NEXAFS will be due to the second layer (Fig 4b). Under this assumption, the azimuthal orientation of the second layer is found to lie between the [001] and [$1\bar{1}0$] directions (twist of 50 ± 15° with respect to the [001] direction).

Assuming that the first layer does indeed coordinate to an undercoordinated surface Ti atom, which seems to be the likely cause of the deprotonation upon adsorption, it then raises the question of the likely adsorption sites of the second layer and the origin of its relatively stable adsorption. One possibility is that the second layer interacts inter-molecularly by forming a hydrogen bond between the first layer N atom that retains its H partner (and is most likely pointing away from the substrate) and the O atoms of the molecules in the second layer. This is indeed the typical mechanism driving the pairing of thymine molecules.[66, 67] In order to probe this possibility, 1-methyluracil was

evaporated onto the TiO_2(110) substrate. This molecule was chosen as the hydrogen atom on the nitrogen atom in position 1 is replaced by a methyl group (see inset of Fig 5b). This methyl group will suppress the ability of the molecule to form hydrogen bonds (assuming the other nitrogen atom is involved in anchoring the molecule to the substrate). After deposition of a sub-monolayer of 1-methyluracil onto the substrate, a line shape similar to the thymine counterpart is observed in the N 1s XPS, with the intensity of the protonated N species again significantly higher than the deprotonated one. Here, it is important to point out that this strong difference in intensity cannot come solely from attenuation of the photoemission signal due to one N atom being closer to the substrate than the other, because the N 1s SXPS data shown in Fig 1a were taken with a photon energy of 550 eV and the TP-XPS data in Fig 1b were taken using a Mg K-α source (hν = 1253.6 eV), resulting in a kinetic energy for the N 1s electrons of ~150 eV and ~850 eV, respectively. This dramatic difference in kinetic energy would result in a strong difference in the inelastic mean free path of the photoelectrons, however, little difference is observed in the XP spectra. Therefore, also for 1-methyluracil the second layer grows spontaneously at a sub-monolayer coverage and in a manner similar to thymine. As 1-methyluracil does not allow the formation of a second layer by means of hydrogen bonding, this suggests that the origin of the second layer lies in the molecule – substrate, rather than intermolecular, interactions. This conclusion is further supported by the results of the crosscheck experiment of Fig 5a (right panel), which shows that the second fully protonated layer forms regardless of whether the outermost N species in the first layer is deprotonated or not. We therefore tentatively suggest that hydrogen bonding between the thymine molecule and the surface leads to the robust anchoring of the second layer. It is possible that this anchoring is between the N-H hydrogen and a surface oxygen, however it is not unreasonable that it is instead a similar interaction between a surface bridging hydroxyl and a thymine carbonyl oxygen (or some mixture of the two). Interactions with these TiO_2 surface hydroxyl species have been found to be a driving force in the dynamics of adsorbed catechol,[68] are suspected to mediate rapid charge transfer between the TiO_2 substrate and adsorbed molecular species,[69] and nucleate the growth of water adlayers.[70] As the adsorption of the first layer of thymine onto TiO_2(110) involves deprotonation, an additional surface hydroxyl species per thymine molecule in the first layer could be created (beside those commonly formed upon water dissociation at bridging oxygen vacancies). Due to the overlap in the binding energy of the thymine and hydroxyl components in the O 1s SXPS (see ESI, Fig. S4), it is not possible to determine unambiguously whether or not such hydroxyl generation does occur, although previous experimental and theoretical evidence regarding deprotonation of carboxylic groups suggests that this should indeed be the case.[27, 71] It is not unreasonable that these hydroxyl species could be stabilising, or even providing the anchoring point for, the second layer of thymine molecules, but lacking a definitive evidence for this interaction we utilise Occam's razor to favour anchoring between the N-H hydrogen and a surface oxygen. Moreover, we note that the coverage of the second layer species is too large to be explained by surface oxygen vacancies (see section 2), and that the greater

twist of the second layer with respect to the [001] direction would suggest that the second layer is not oriented along the surface Ti row.

Finally, considering model adsorption sites for the first layer thymine, placing a nitrogen atom above an undercoordinated surface Ti atom would bring the two carbonyl O atoms of thymine close to planar surface O atoms, given the 30° twist indicated by NEXAFS. This is illustrated in Fig 6, where five-fold coordinated Ti atoms and the surrounding planar O atoms are indicated. It therefore seems more likely that the deprotonated N atom is located in a site that bridges two adjacent Ti atoms, placing the carbonyl O atoms in off atop sites (as seen in Fig 6) – this adsorption site would be counter to that observed on Cu(110). However, without a technique that is sensitive to the local adsorption, such assignment is rather speculative. As to the N species that first undergoes deprotonation in the first layer, the analogy with adsorbed thymine and uracil on Cu(110)[39, 41] and Cu(111)[72] suggests that this is the N atom in position 3 (inset of Fig 1c) between the two carbonyl groups (note, however, that cytosine on Cu(110) is known to coordinate through the other nitrogen atom, N(1), in the pyrimidine ring[42]). Although this assertion cannot be proved unambiguously based on our data, the C 1s SXPS results of Fig 1c support such conclusion. In fact, the 1 eV shift in binding energy between the two first-layer carbonyl C 1s components agrees well with C 1s gas-phase data[63] and, together with the almost rigid shift upon annealing from 300 K to 450 K, points towards a similar interaction of the two species with the underlying surface. Moreover, a single O 1s XPS peak at about 532 eV characterizes the first layer (Fig S4 in the ESI), further corroborating a symmetric configuration of the two carbonyl oxygens on the surface, as ensured by anchoring through the deprotonated N(3) atom.

5. Conclusions

The adsorption of thymine on the (110) termination of rutile titanium dioxide was investigated by a joint SXPS, TP-XPS, NEXAFS and TPD study. The results suggest a bilayer adsorption motif, with the molecules in the first layer azimuthally rotated by 30±10° off the [001] direction and those in the second layer rotated by 50±15°. Both layers are mostly upright, with a 30±10° tilt of the molecules with respect to the surface normal and the species in the first layer singly deprotonated upon N-H bond cleavage. N 1s XPS measurements of 1-methyl uracil on the same surface indicate that the origin of the bilayer structure is not intermolecular hydrogen bonding, implying that it is presumably mediated by the interaction with the undercoordinated bridging oxygen rows of the surface. The orientation and tilt of the first layer suggest that the most likely adsorption configuration has one of the two nitrogen atoms of the thymine molecules bridging the undercoordinated surface Ti atoms. This would, in turn, suggest that the second layer adsorbs with the hydrogen atom of one of the two N atoms coordinated above an undercoordinated surface O atom. For this reason, what we have

described as a bilayer could equivalently be considered as a strongly corrugated saturated layer with two chemically-distinct molecular species adsorbed in two different sites (and configurations), as dictated by the pronounced geometric and electronic corrugation of the TiO_2(110) surface.

This finding of a thermally stable, highly corrugated adsorption geometry suggests intriguing potential for the targeted functionalisation of TiO_2 by the adsorption of simple biomolecules. The duality of the nature of the adsorption, and the discovery that intermolecular interactions are not driving this corrugation of the adsorption geometry, suggests that the nitrogen atom not taking part in the coordination of the molecule to the substrate can still be utilised for interaction with other polar species. This potential polar template could provide two geometrically unique, but electronically similar sites (a pyrimidinic NH species) for additional adducts to interact with. However, this raises one of the major remaining questions in this system – whether the thymine coordinates to the substrate through the N(1) nitrogen (the same nitrogen atom through which thymine binds in its nucleoside) or the N(3) nitrogen (as we suggested for the first layer). If the former, this template could provide a similar binding environment on a local scale as the nucleobase does within DNA; if the latter, this template could provide a novel bonding environment. In both cases, however, this template could offer a stable bonding environment for other nucleobases, most notably thymine's paired base adenine, and amino acids.

Acknowledgements

This work was supported by the European Research Council (ERC Advanced Grant MolArt no. 247299), the Munich Centre for Advanced Photonics (MAP, projects B.1.3 and B.1.4.) funded by the German Research Foundation (DFG) via the German Excellence Initiative. In addition, the research leading to the above presented results has received funding from the European Community's Seventh Framework Programme (FP7/2007-2013) CALIPSO under grant agreement nº 312284. D.A.D. would like to acknowledge funding from the Alexander von Humboldt Foundation and a Marie Curie intra-European Fellowship (Project Silinano). Experimental support of K. C. Prince at the Materials Science beam line, and Karina Schulte and Jacek Osiecki at I311 beam line is also gratefully acknowledged.

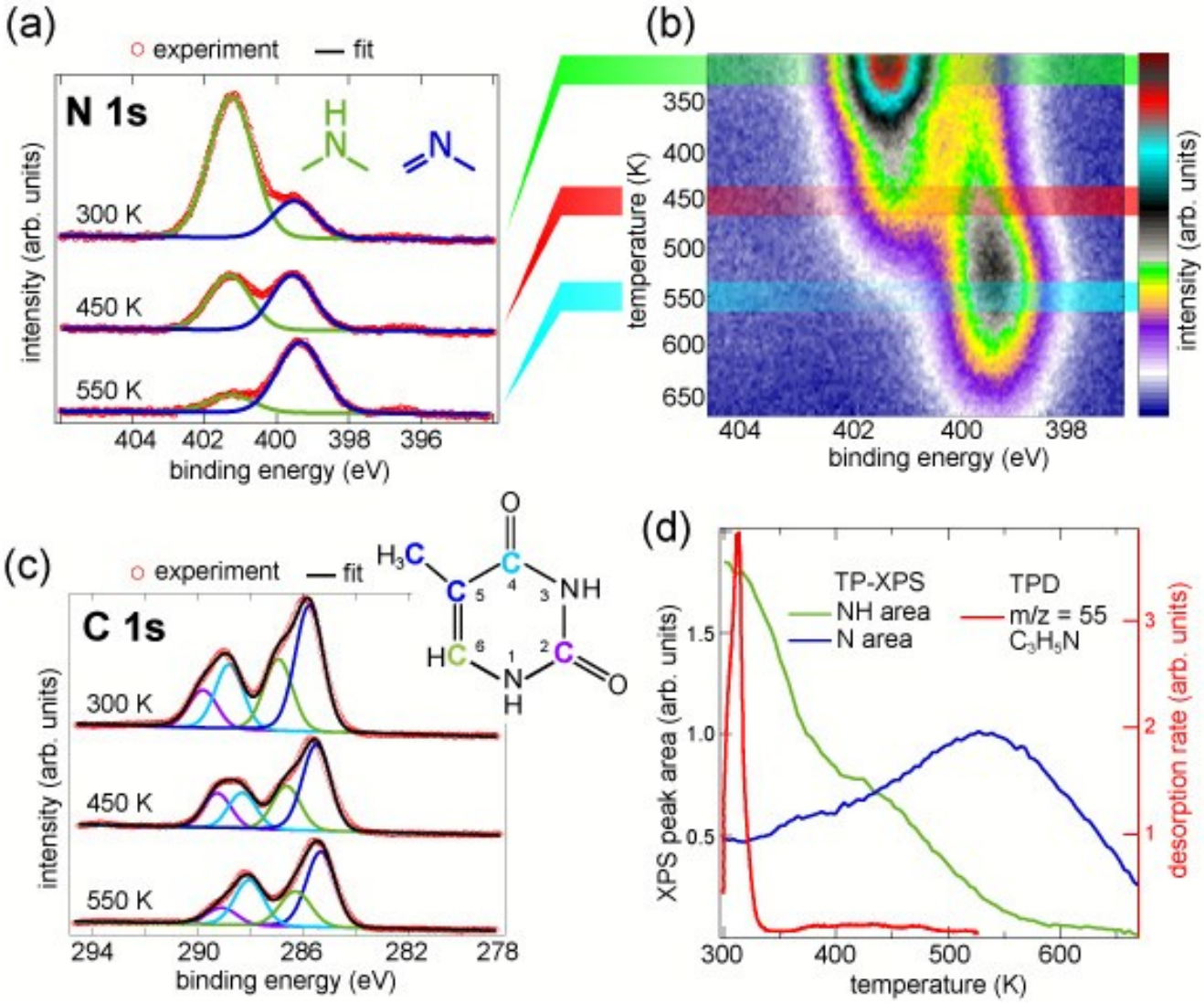

Figure 1. (a) N 1s SXPS (hv = 550 eV) acquired at room temperature after thymine deposition at 300 K, after annealing to 450 K, and after annealing to 550 K; the peak assignments are indicated by the inset schematic showing a protonated and deprotonated N species. (b) N 1s TP-XPS (hv = 1253.6 eV) measured at a constant heating rate of 0.1 K/s. (c) C 1s SXPS (hv = 435 eV) measured under the same conditions as the N 1s SXPS. The peak assignment is indicated by the colouring of the inset schematic of the thymine molecule and was performed in agreement with Ref. [63], accounting for a ~5.4 eV (almost rigid) binding energy shift due to work function correction and core-hole screening from the TiO_2(110) substrate. (d) Fitted peak areas of the N 1s TP-XPS for the protonated and deprotonated N species compared against the mass 55 amu desorption rate determined from TPD at the same heating rate (0.1 K/s). Mass 55 amu represents a characteristic fragment of thymine.[60]

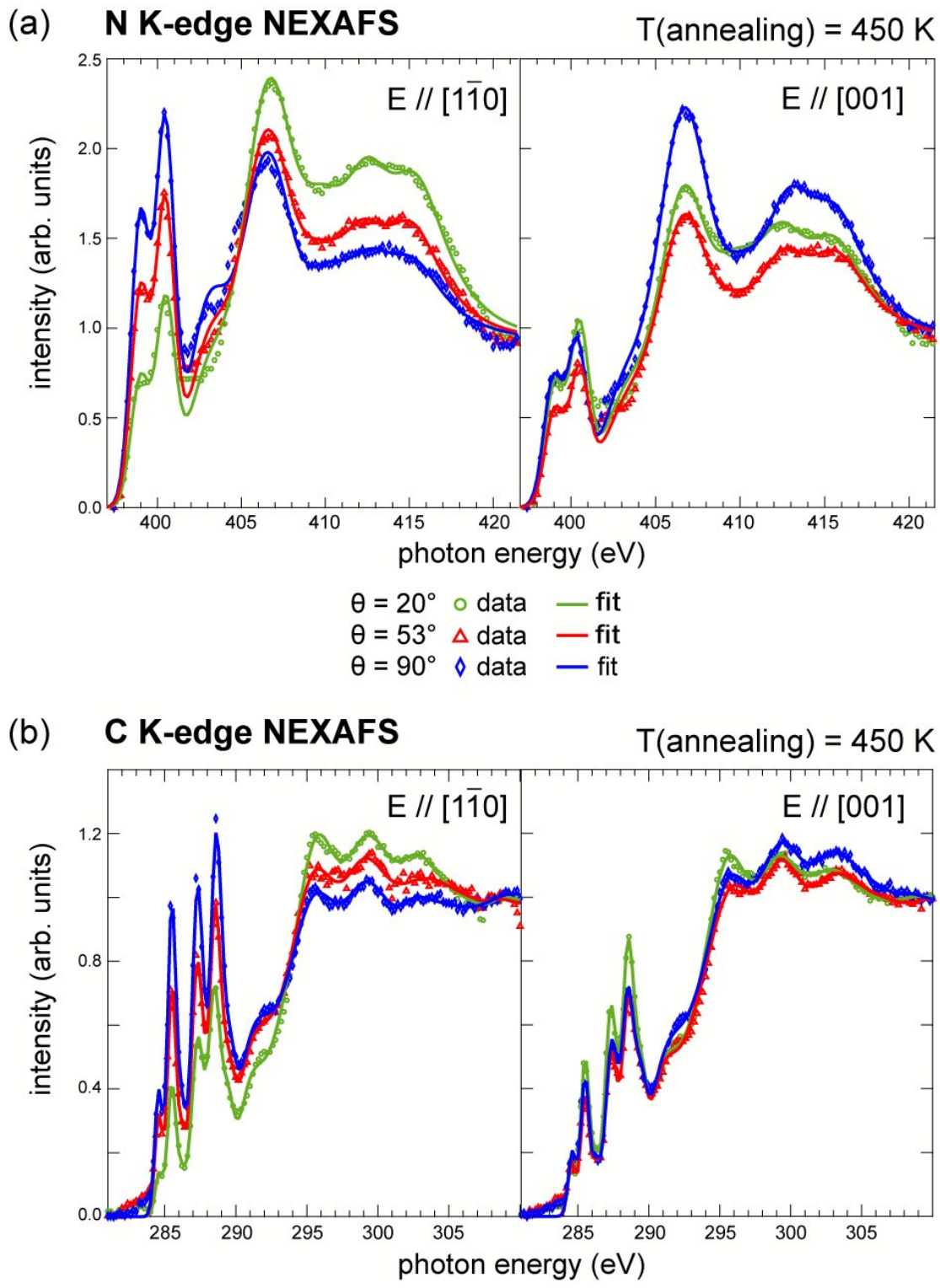

Figure 2. (a) N K-edge and (b) C K-edge NEXAFS acquired at room temperature from a saturated thymine layer on TiO_2(110) after annealing to 450 K. Exemplary fits for the N K-edge, including the individual fitting components, are shown in the ESI (Fig S1). Θ is the angle between the photon polarisation (E) and the surface normal.

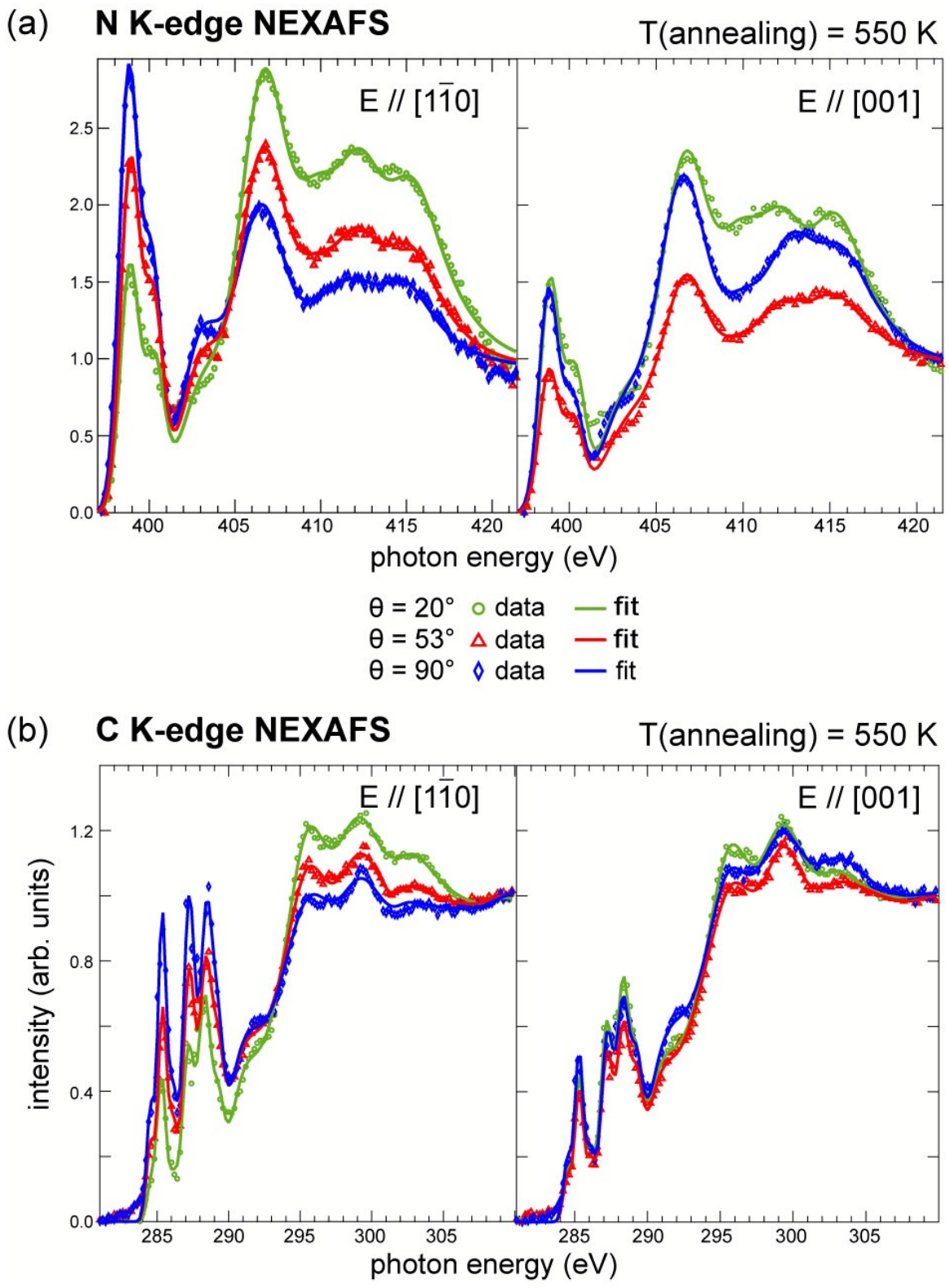

Figure 3. (a) N K-edge and (b) C K-edge NEXAFS acquired at room temperature from a saturated thymine layer on TiO_2(110) after annealing to 550 K. Exemplary fits for the N K-edge, including the individual fitting components, are shown in the ESI (Fig S2). Θ is the angle between the photon polarisation (E) and the surface normal.

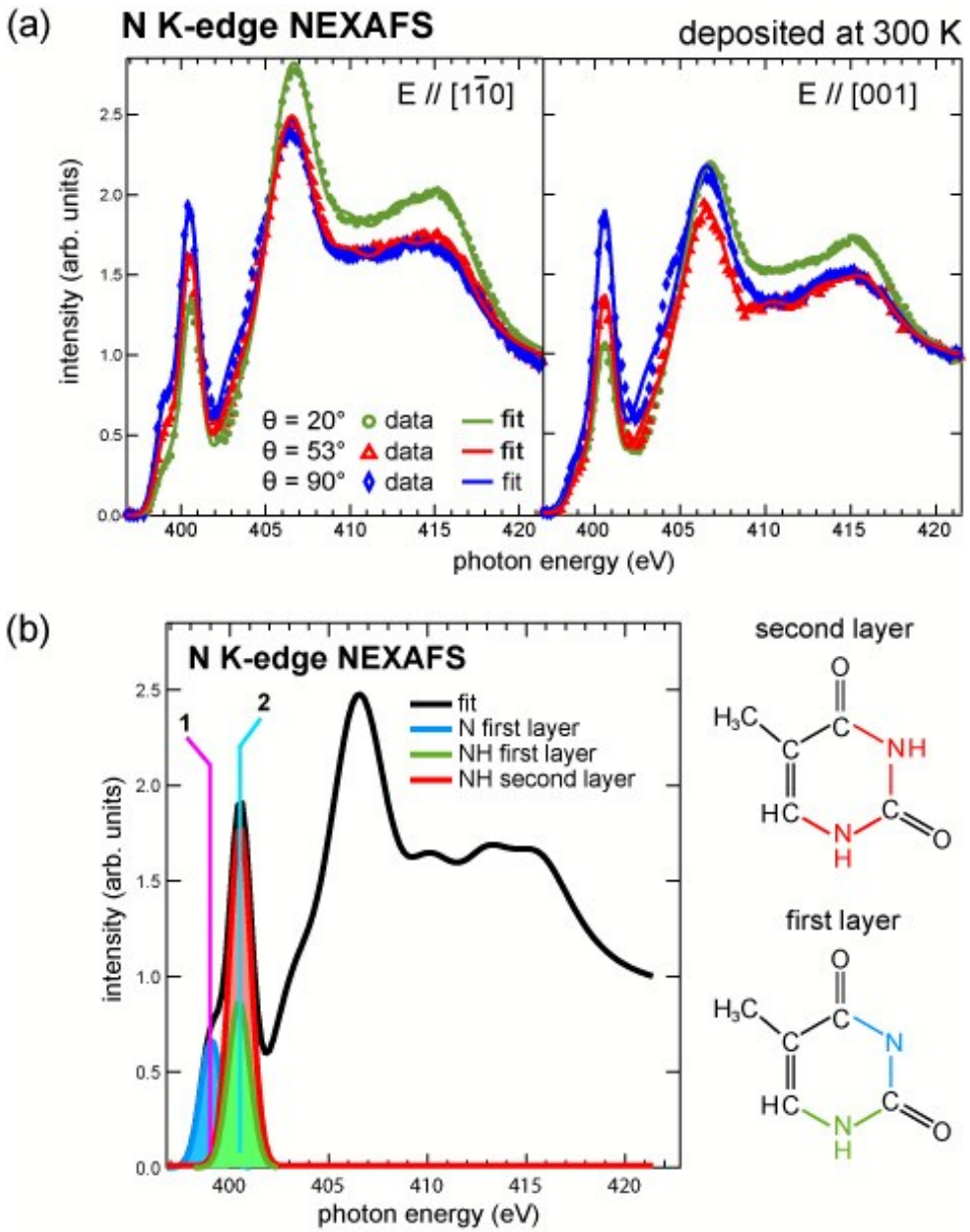

Figure 4. (a) N K-edge NEXAFS acquired at room temperature from a saturated thymine layer on TiO_2(110). Exemplary fits for the N K-edge, including the individual fitting components, are shown in the ESI (Fig S3). Θ is the angle between the photon polarisation (E) and the surface normal. (b) A schematic of the deconvolution of peak 2 (indicated by the cyan line) into a contribution from the first layer (green peak) and the second layer (red peak), based on the intensity of peak 1 (pink line) that has only a contribution from the first layer (blue peak). The assignment of the features is indicated by the colouring of the molecular schematic (on the right). The ratio of the intensity between the two different N atoms in the first layer is assumed to share the same ratio as in Fig 2. From the here presented data it is not possible to unambiguously assign which nitrogen atom is deprotonated, but it is likely that it is the nitrogen atom that lies between the two carbonyl groups, as was found for thymine and uracil on Cu(110).[39, 41]

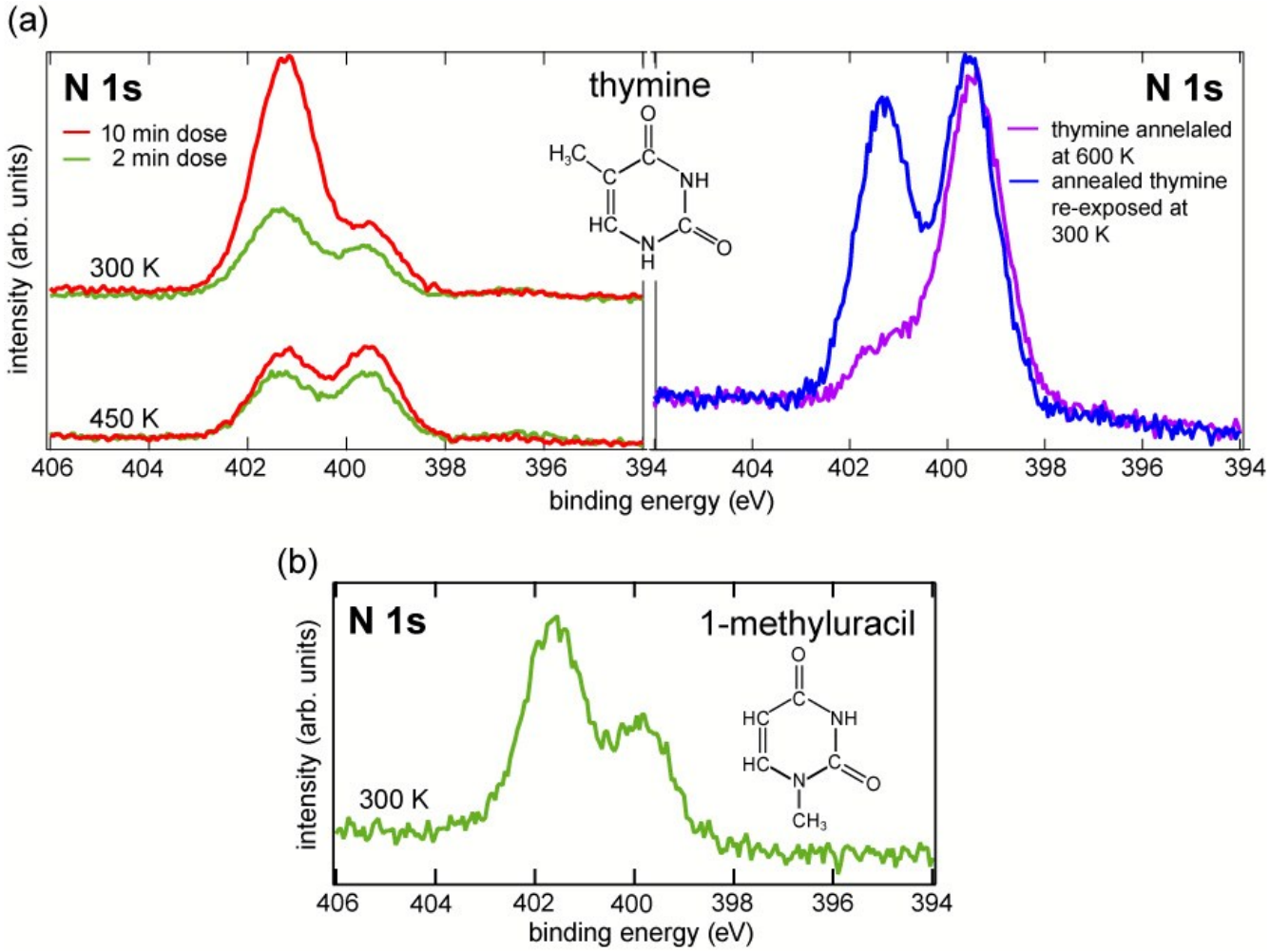

Figure 5. (a, left) N 1s SXPS (hv = 550 eV) comparing a saturated and sub-monolayer exposure (10 min and 2 min of exposure, respectively) of TiO_2(110) to thymine (300 K); also shown are the same preparations after annealing to 450 K. (a, right) A preparation similar to the 10 min dose after annealing to 600 K compared to a subsequent saturation exposure of the annealed system to more thymine. (b) N 1s XPS (hv = 1253.6 eV) after a sub-monolayer exposure of the TiO_2(110) surface to 1-methyluracil (molecular structure shown schematically in the inset). All measurements in panels (a) and (b) were performed at room temperature.

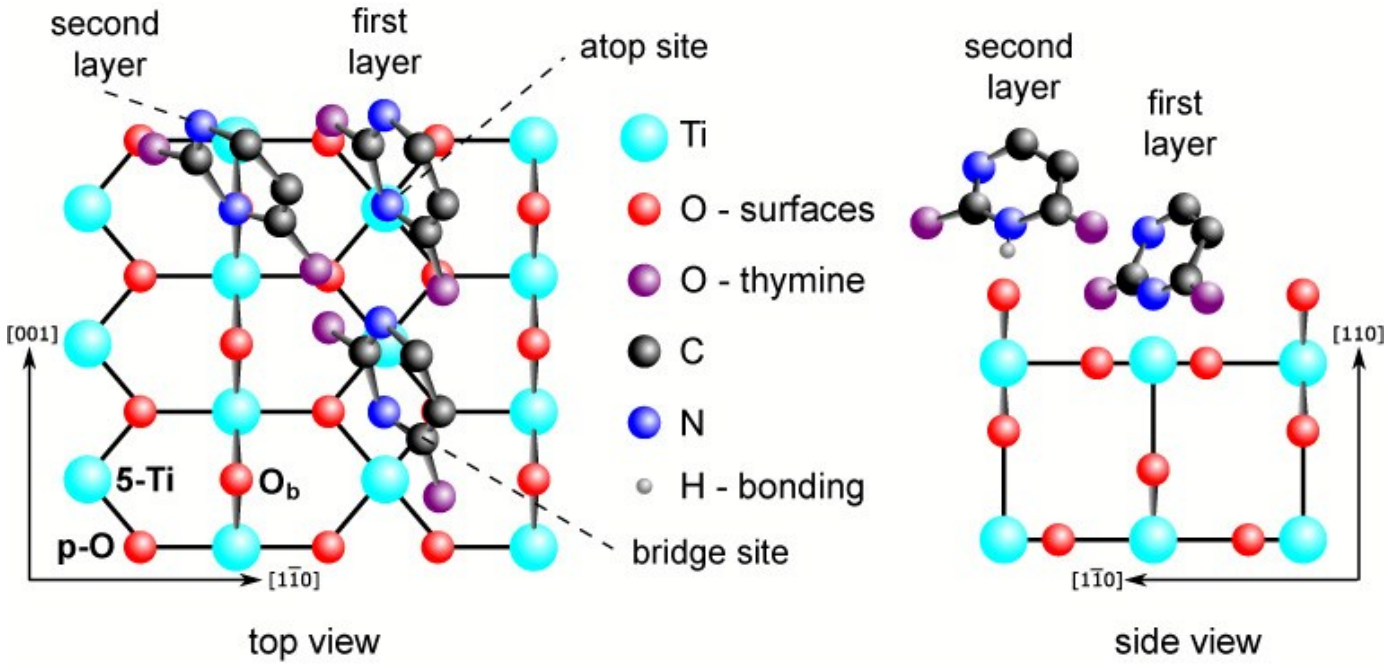

Figure 6. A schematic of the potential adsorption sites of a first thymine layer molecule (singly deprotonated) on TiO_2(110), assuming it coordinates either bridging or directly atop a surface Ti atom, viewed along the substrate's (left) [110] and (right) [001] directions. Also shown is the proposed adsorption site of an individual molecule in the second layer of fully protonated thymine above a surface oxygen atom. In both cases, it is assumed that the molecule coordinates through the nitrogen atom that lies between the two carbonyl groups, similar to thymine and uracil on Cu(110), [39, 41] although it is important to note that cytosine (also on Cu(110)) coordinates through the other nitrogen atom in the pyrimidine ring.[42] In the tentative models, the H atoms (excluding the H atom through which the second layer interacts with the substrate) and the thymine methyl group are not shown for the sake of clarity. The undercoordinated Ti atoms (5-Ti), the planarly coordinated O atoms (p-O) and the protruding bridging oxygen atoms (O_b) of the rutile (110) surface are highlighted in the bottom part of the left panel. The formation and possible role of adjacent hydroxyl groups on the O_b rows, as discussed in the text, are not addressed in the schematics.

Table 1: Twist and tilt angles, given with respect to the [001] surface direction and the surface normal (respectively), determined from the N K-edge and C K-edge NEXAFS data (respectively). Specifically, the angles are reported for the "monolayer" (Fig 2), the "doubly deprotonated" monolayer (Fig 3), and the "bilayer" (Fig 4). The bilayer angles are separated into the angle found for the lower photon energy (lower hv) species, the higher photon energy (higher hv) species and the angle for the second layer ("deconvoluted") that was determined as by Fig 4b.

		monolayer 450 K	deprotonated 550 K	bilayer lower hv 300 K	bilayer higher hv 300 K	bilayer deconvoluted 300 K
N K-edge	twist	30±10°	30±10°	30±10°	40±10°	50±15°
	tilt	30±10°	30±10°	30±10°	30±10°	--
C K-edge	twist	30±10°	30±10°	--	--	--
	tilt	30±10°	30±10°	--	--	--

References:

1. B. Kasemo, *Surf. Sci.*, 2002, **500**, 656-677.
2. T. Qiu and M. A. Barteau, *J. Colloid Interface Sci.*, 2006, **303**, 229-235.
3. Z. Pászti, T. Keszthelyi, O. Hakkel and L. Guczi, *J. Phys.: Condens. Matter*, 2008, **20**, 224014.
4. S. Köppen, O. Bronkalla and W. Langel, *J. Phys. Chem. C*, 2008, **112**, 13600-13606.
5. G. J. Fleming, K. Adib, J. A. Rodriguez, M. A. Barteau, J. M. White and H. Idriss, *Surf. Sci.*, 2008, **602**, 2029-2038.
6. S. Monti, V. Carravetta, C. Battocchio, G. Iucci and G. Polzonetti, *Langmuir*, 2008, **24**, 3205-3214.
7. T. J. Lerotholi, E. A. Kröger, M. J. Knight, W. Unterberger, K. Hogan, D. C. Jackson, C. L. A. Lamont and D. P. Woodruff, *Surf. Sci.*, 2009, **603**, 2305-2311.
8. R. Tonner, *ChemPhysChem*, 2010, **11**, 1053-1061.
9. S. Monti, A. C. T. van Duin, S.-Y. Kim and V. Barone, *J. Phys. Chem. C*, 2012, **116**, 5141-5150.
10. M. J. Tillotson, P. M. Brett, R. A. Bennett and R. Grau-Crespo, *Surf. Sci.*, 2015, **632**, 142-153.
11. M. Schmidt and S. G. Steinemann, *Fresenius J. Anal. Chem.*, 1991, **341**, 412-415.
12. S. G. Steinemann, *Periodontology 2000*, 1998, **17**, 7-21.
13. G. J. Fleming, K. Adib, J. A. Rodriguez, M. A. Barteau and H. Idriss, *Surf. Sci.*, 2007, **601**, 5726-5731.
14. T. Hanawa, *J. Periodontal Implant Sci.*, 2011, **41**, 263-272.
15. C. Lun Pang, R. Lindsay and G. Thornton, *Chem. Soc. Rev.*, 2008, **37**, 2328-2353.
16. T. Albaret, F. Finocchi and C. Noguera, *Faraday Discuss.*, 1999, **114**, 285-304.
17. A. T. Paxton and L. Thiên-Nga, *Phys. Rev. B*, 1998, **57**, 1579-1584.
18. H. Iddir, S. Öğüt, N. D. Browning and M. M. Disko, *Phys. Rev. B*, 2005, **72**, 081407.
19. M. Blanco-Rey, J. Abad, C. Rogero, J. Mendez, M. F. Lopez, J. A. Martin-Gago and P. L. de Andres, *Phys. Rev. Lett.*, 2006, **96**, 055502.
20. S. C. Jensen, A. Shank, R. J. Madix and C. M. Friend, *ACS Nano*, 2012, **6**, 2925-2930.
21. S.-C. Li, J.-g. Wang, P. Jacobson, X. Q. Gong, A. Selloni and U. Diebold, *J. Am.*

Chem. Soc., 2009, **131**, 980-984.

22. J. Schütte, R. Bechstein, P. Rahe, M. Rohlfing, A. Kühnle and H. Langhals, *Phys. Rev. B*, 2009, **79**, 045428.
23. P. Rahe, M. Nimmrich, A. Nefedov, M. Naboka, C. Wöll and A. Kühnle, *J. Phys. Chem. C*, 2009, **113**, 17471-17478.
24. S.-C. Li and U. Diebold, *J. Am. Chem. Soc.*, 2010, **132**, 64-66.
25. D. C. Grinter, T. Woolcot, C.-L. Pang and G. Thornton, *J. Phys. Chem. Lett.*, 2014, **5**, 4265-4269.
26. G. Otero-Irurueta, J. I. Martínez, G. Lovat, V. Lanzilotto, J. Méndez, M. F. López, L. Floreano and J. A. Martín-Gago, *J. Phys. Chem. C*, 2015, **119**, 7809-7816.
27. D. I. Sayago, M. Polcik, R. Lindsay, R. L. Toomes, J. T. Hoeft, M. Kittel and D. P. Woodruff, *J. Phys. Chem. B*, 2004, **108**, 14316-14323.
28. F. Allegretti, S. O'Brien, M. Polcik, D. I. Sayago and D. P. Woodruff, *Phys. Rev. Lett.*, 2005, **95**, 226104.
29. D. A. Duncan, F. Allegretti and D. P. Woodruff, *Phys. Rev. B*, 2012, **86**, 045411.
30. A. G. Thomas and K. L. Syres, *Chem. Soc. Rev.*, 2012, **41**, 4207-4217.
31. D. Kreikemeyer-Lorenzo, W. Unterberger, D. A. Duncan, T. J. Lerotholi and D. P. Woodruff, *Surf. Sci.*, 2013, **613**, 40-47.
32. M. J. Jackman, K. L. Syres, D. J. H. Cant, S. J. O. Hardman and A. G. Thomas, *Langmuir*, 2014, **30**, 8761-8769.
33. S. Kilina, S. Tretiak, D. A. Yarotski, J.-X. Zhu, N. Modine, A. Taylor and A. V. Balatsky, *J. Phys. Chem. C*, 2007, **111**, 14541-14551.
34. C. Desfrançois and J. P. Schermann, in *Atomic and Molecular Beams: The State of the Art 2000*, ed. R. Campargue, Springer Berlin Heidelberg, 2001, DOI: 10.1007/978-3-642-56800-8_56, pp. 815-825.
35. C. Desfrançois, H. Abdoul-Carime, N. Khelifa and J. P. Schermann, *Phys. Rev. Lett.*, 1994, **73**, 2436-2439.
36. J. Liu, L. de la Garza, L. Zhang, N. M. Dimitrijevic, X. Zuo, D. M. Tiede and T. Rajh, *Chem. Phys.*, 2007, **339**, 154-163.
37. R. Smoluchowski, *Phys. Rev.*, 1941, **60**, 661-674.
38. A. Liebsch, J. Harris, B. Salanon and J. Lapujoulade, *Surf. Sci.*, 1982, **123**, 338-354.
39. F. Allegretti, M. Polcik and D. P. Woodruff, *Surf. Sci.*, 2007, **601**, 3611-3622.
40. I. Temprano, G. Thomas, S. Haq, M. S. Dyer, E. G. Latter, G. R. Darling, P. Uvdal and R. Raval, *J. Chem. Phys.*, 2015, **142**, 101916.
41. D. A. Duncan, W. Unterberger, D. Kreikemeyer-Lorenzo and D. P. Woodruff, *J.*

Chem. Phys., 2011, **135**, 014704.

42. D. C. Jackson, D. A. Duncan, W. Unterberger, T. J. Lerotholi, D. K. Lorenzo, M. K. Bradley and D. P. Woodruff, *J. Phys. Chem. C*, 2010, **114**, 15454-15463.
43. M. Pascal, C. L. A. Lamont, M. Kittel, J. T. Hoeft, R. Terborg, M. Polcik, J. H. Kang, R. Toomes and D. P. Woodruff, *Surf. Sci.*, 2001, **492**, 285-293.
44. A. Puschmann, J. Haase, M. D. Crapper, C. E. Riley and D. P. Woodruff, *Phys. Rev. Lett.*, 1985, **54**, 2250-2252.
45. D. Kreikemeyer-Lorenzo, W. Unterberger, D. A. Duncan, M. K. Bradley, T. J. Lerotholi, J. Robinson and D. P. Woodruff, *Phys. Rev. Lett.*, 2011, **107**, 046102.
46. A. Wu, T. Paunesku, E. M. B. Brown, A. Babbo, C. Cruz, M. Aslam, V. Dravid and G. E. Woloschak, *Nano*, 2008, **03**, 27-36.
47. H. Arora, C. Doty, Y. Yuan, J. Boyle, K. Petras, B. Rabatic, T. Paunesku and G. Woloschak, in *Nanomaterials for the Life Sciences*, ed. C. S. S. R. Kumar, Wiley-VCH Verlag GmbH & Co. KGaA, Weinheim, 2010, vol. 8: Nanocomposites, ch. 1.
48. F. M. Kievit and M. Zhang, *Acc. Chem. Res.*, 2011, **44**, 853-862.
49. A. S. Levina, M. N. Repkova, Z. R. Ismagilov, N. V. Shikina, E. G. Malygin, N. A. Mazurkova, V. V. Zinov'ev, A. A. Evdokimov, S. I. Baiborodin and V. F. Zarytova, *Sci. Rep.*, 2012, **2**, 756.
50. Y. Yin, W.-W. Zhu, L.-P. Guo, R. Yang, X.-S. Li and Y. Jiang, *J. Phys. Chem. B*, 2013, **117**, 125-131.
51. R. Bazak, J. Ressl, S. Raha, C. Doty, W. Liu, B. Wanzer, S. A. Salam, S. Elwany, T. Paunesku and G. E. Woloschak, *Nanoscale*, 2013, **5**, 11394-11399.
52. R. M. Fratila, S. G. Mitchell, P. del Pino, V. Grazu and J. M. de la Fuente, *Langmuir*, 2014, **30**, 15057-15071.
53. J. Conde, J. T. Dias, V. Grazú, M. Moros, P. V. Baptista and J. M. de la Fuente, *Front. Chem.*, 2014, **2**, 48.
54. Q. Yuan, Z. Wu, Y. Jin, F. Xiong and W. Huang, *J. Phys. Chem. C*, 2014, **118**, 20420-20428.
55. S. P. Frigo, P. Feulner, B. Kassühlke, C. Keller and D. Menzel, *Phys. Rev. Lett.*, 1998, **80**, 2813-2816.
56. U. Diebold and T. E. Madey, *Surf. Sci. Spectra*, 1996, **4**, 227-231.
57. M. Oku, K. Wagatsuma and S. Kohiki, *Phys. Chem. Chem. Phys.*, 1999, **1**, 5327-5331.
58. F. Allegretti, J. P. W. Treacy and R. Lindsay, *Phys. Rev. B*, 2012, **85**, 205422.
59. U. Diebold, *Surf. Sci. Rep.*, 2003, **48**, 53-229.
60. National Institute of Standards and Technology (NIST) - Reference

Data, http://webbook.nist.gov/cgi/cbook.cgi?ID=C65714&Mask=200#Mass-Spec).

61. G. G. Fuentes, E. Elizalde, F. Yubero and J. M. Sanz, *Surf. Interface Anal.*, 2002, **33**, 230-237.
62. Atomic Calculation of Photoionization Cross-Sections and Asymmetry Parameters - Elettra Web Page, https://vuo.elettra.eu/services/elements/WebElements.html).
63. O. Plekan, V. Feyer, R. Richter, M. Coreno, M. de Simone, K. C. Prince, A. B. Trofimov, E. V. Gromov, I. L. Zaytseva and J. Schirmer, *Chem. Phys.*, 2008, **347**, 360-375.
64. J. Stöhr, *NEXAFS Spectroscopy*, Springer-Verlag, 2003.
65. J. Stöhr and D. A. Outka, *Phys. Rev. B*, 1987, **36**, 7891-7905.
66. R. E. A. Kelly and L. N. Kantorovich, *J. Phys. Chem. B*, 2006, **110**, 2249-2255.
67. W. Xu, R. E. A. Kelly, R. Otero, M. Schöck, E. Lægsgaard, I. Stensgaard, L. N. Kantorovich and F. Besenbacher, *Small*, 2007, **3**, 2011-2014.
68. S.-C. Li, L.-N. Chu, X.-Q. Gong and U. Diebold, *Science*, 2010, **328**, 882-884.
69. K. Onda, B. Li, J. Zhao, K. D. Jordan, J. Yang and H. Petek, *Science*, 2005, **308**, 1154-1158.
70. G. Ketteler, S. Yamamoto, H. Bluhm, K. Andersson, D. E. Starr, D. F. Ogletree, H. Ogasawara, A. Nilsson and M. Salmeron, *J. Phys. Chem. C*, 2007, **111**, 8278-8282.
71. W. Busayaporn, D. A. Duncan, F. Allegretti, A. Wander, M. Bech, P. J. Møller, B. P. Doyle, N. M. Harrison, G. Thornton and R. Lindsay, *J. Phys. Chem. C*, 2016, DOI: 10.1021/acs.jpcc.6b03991.
72. A. C. Papageorgiou, S. Fischer, J. Reichert, K. Diller, F. Blobner, F. Klappenberger, F. Allegretti, A. P. Seitsonen and J. V. Barth, *ACS Nano*, 2012, **6**, 2477-2486.